Chemically Induced Magnetism and Magnetoresistance in $La_{0.8}Sr_{1.2}Mn_{0.6}Rh_{0.4}O_4$

Peter D. Battle,*,† Anthony M. T. Bell,† Stephen J. Blundell,‡ Amalia I. Coldea,‡ Edmund J. Cussen,§ Georgina C. Hardy,§ Ishbel M. Marshall,‡ Matthew J. Rosseinsky,*,§ and Christopher A. Steer‡

Contribution from the Inorganic Chemistry Laboratory, Chemistry Department, University of Oxford, South Parks Road, Oxford OX1 3QR, U.K., Clarendon Laboratory, Department of Physics, University of Oxford, Parks Road, Oxford OX1 3PU, U.K., and Department of Chemistry, University of Liverpool, Liverpool L69 7ZD, U.K.

Received April 13, 2001

Abstract: It is shown by magnetometry and μSR spectroscopy that short-range magnetic interactions between the Mn cations in the nonmetallic K_2NiF_4-like phase $La_{0.8}Sr_{1.2}Mn_{0.6}Rh_{0.4}O_4$ become significant below ~200 K. Negative magnetoresistance ($\rho/\rho(0) \sim 0.5$ in 14 T at 108 K) is apparent below this temperature. Neutron diffraction has shown that an applied magnetic field of 5 T is sufficient to induce saturated ($3.38(7)\mu_B$ per Mn) long-range ferromagnetic ordering of the atomic moments at 2 K, and that the induced ordering persists up to a temperature of 50 K in 5 T. Spin glass behavior is observed below 20 K in the absence of an applied field. The induced magnetic ordering is attributed to the subtle changes in band structure brought about by the external field, and to the controlling influence of Rh^{3+} over the relative strength of competing magnetic exchange interactions.

There has been a resurgence of interest in ferromagnetic oxides due to the strong coupling between spin ordering and charge transport found in the $La_{1-x}Sr_xMnO_3$ perovskites which display colossal magnetoresistance (MR).[1] The reduction of the zero-field resistance in an applied field can be as large as $\Delta\rho/\rho(H=0) = 0.999$ in fields of over 50 kOe, but achieving significant MR in the low fields required for information storage applications has proved a difficult barrier for the current generation of materials. Increasing attention is now being paid [2,3] to perovskites in which the Mn site is doped with a second transition element, for example Cr or Ru, and to the intrinsically layered members of the Ruddlesden−Popper (RP) $A_{n+1}B_nO_{3n+1}$ series, for example $n = 2La_{1.8}Sr_{1.2}Mn_2O_7$, which display MR in fields as low as 3 kOe because the barrier to the field aligning the magnetization between the perovskite blocks in the layer stacking sequence is small. Unfortunately, the required ferromagnetism has not yet been found in the two-dimensional $Sr_{1+x}La_{1-x}MnO_4$ $n = 1$ member of the RP series, with the Sr_2MnO_4 and $LaSrMnO_4$ end-members being antiferromagnets while the $Mn^{III/IV}$ solid solutions are spin glasses. We have, however, previously reported[4] that substitution of formally diamagnetic Rh(III) into $Sr_{1.2}La_{0.8}MnO_4$ produces a material with short-range spin ordering in zero field which achieves a moment of 2.50 μ_B per manganese in a 50 kOe field. The introduction of the diamagnetic second series transition metal thus has a more dramatic electronic effect than that expected on the basis of simple magnetic dilution arguments, suggesting that significant electronic interactions are induced by the mixing of Rh 4d orbitals with the electronically active 3d orbitals of Mn. A detailed understanding of the electronic effects of this simple substitutional chemistry requires the application of techniques capable of probing both the statics and the dynamics of the Mn spin system and we describe below a more detailed investigation by μSR and neutron diffraction. We show that $La_{0.8}Sr_{1.2}Mn_{0.6}Rh_{0.4}O_4$ (mean oxidation state of Mn = 3.33) achieves long-range ferromagnetic order in an applied magnetic field at low temperatures, whereas spin-glass behavior persists in zero field. We conclude that the electron configuration of the diamagnetic dopant is crucial in determining the properties of the material.

Experimental Section

Three samples of $La_{0.8}Sr_{1.2}Mn_{0.6}Rh_{0.4}O_4$, referred to as E, G, and T, were used in this study. The preparation, structural chemistry, and magnetic properties of sample G have been described previously.[4] The desire to eliminate the small concentration (0.5% by mass) of an La_2O_3 impurity in sample G prompted the preparation of samples E and T. The preparation of sample E followed the protocol for sample G, albeit with an additional 3 days of firing at 1523 K. Sample T was prepared by heating a stoichiometric mixture of $SrCO_3$, MnO_2, La_2O_3, and Rh_2O_3 at 1073 K for 4 days and then at 1273 K for 2 days in pellet form. Further heat treatments were carried out at 1473 (5 days) and 1523 K (1 day) with regular regrinding and pelletizing. The initial reaction products were black powders which were shown by X-ray powder diffraction to contain a K_2NiF_4-type phase and unreacted La_2O_3; the latter was gradually eliminated during the course of the reaction. X-ray powder diffraction patterns of the final products were recorded using Cu $K\alpha_1$ radiation over the angular range $10 \leq 2\theta/\text{deg} \leq 120$ with a step size of $\Delta 2\theta = 0.02°$. The magnetic susceptibility of samples T and E was measured on warming through the temperature range $5 \leq$

† Oxford Chemistry.
‡ Oxford Physics.
§ University of Liverpool.

(1) Ramirez, A. P. *J. Phys.: Condens. Matter* **1997**, *9*, 8171.
(2) Raveau, B.; Hervieu, M.; Maignan, A.; Martin, C. *J. Mater. Chem.* **2001**, *11*, 29.
(3) Battle, P. D.; Rosseinsky, M. J. *Curr. Opin. Solid State Mater. Sci.* **1999**, *4*, 163.
(4) Battle, P. D.; Burley, J. C.; Cussen, E. J.; Hardy, G. C.; Hayward, M. A.; Noailles, L. D.; Rosseinsky, M. J. *Chem. Commun.* **1999**, 1977.

10.1021/ja010958+ CCC: $20.00
Published on Web 07/13/2001

Table 1. Structural Parameters for $La_{0.8}Sr_{1.2}Mn_{0.6}Rh_{0.4}O_4$ at 290 K[a]

sample	*a* (Å)	*c* (Å)	*z* (Sr/La)	*z* (O1)	Mn/Rh−O1 (Å)	Mn/Rh−O2 (Å)	χ^2
T	3.8904(6)	12.514(2)	0.3588(1)	0.1649(1)	2.064(2)	1.9452(3)	1.6
E	3.8909(6)	12.521(2)	0.35843(8)	0.1648(1)	2.063(2)	1.9454(3)	1.8
G	3.88641(8)	12.5144(3)	0.35864(7)	0.1646(1)	2.060(1)	1.94321(4)	2.8

[a] Space group *I*4/*mmm*, Sr/La on 0,0,*z*; Mn/Rh on 0,0,0; O1 on 0,0,*z*; O2 on $^1/_2$,0,0.

T/K ≤ 300 in an applied magnetic field of 100 Oe using a Quantum Design MPMS SQUID magnetometer, the sample being contained in a gelatin capsule; data were collected after cooling in zero field (ZFC) and after cooling in the measuring field (FC). The magnetization of each sample was measured as a function of field ($0 \le H$/kOe ≤ 50) at temperatures selected in light of the results of our magnetoresistance measurements. These were carried out on a sintered bar using a four-terminal method with a direct current of less than 10 μA. The sample was mounted in a variable-temperature insert which was loaded into a 17 T superconducting magnet. The magnetic field was applied perpendicular to the current direction. Muon-spin relaxation (μSR) data were taken on the EMU pulsed muon beam-line at the ISIS facility at the Rutherford Appleton Laboratory. In our μSR experiments,[5] a beam of almost completely spin polarized muons was implanted with a momentum of 28 MeV/c into the sample under investigation. The muons stop quickly (in $<10^{-9}$ s), without significant loss of polarization. The observed quantity is the time evolution of the muon spin polarization, which depends on the distribution of internal magnetic fields and their temporal fluctuations, and which can be measured by counting emitted decay positrons forward and backward of the initial muon spin direction; this is possible owing to the asymmetric nature of the muon decay, which takes place in a mean time of 2.2 μs. For the zero-field muon experiments, the background magnetic field was compensated to be less than 10 μT. Time-of-flight neutron powder diffraction data were collected on both of these samples over the *d*-spacing range $0.29 \le$ d/Å ≤ 6.8 at room temperature using the instrument GEM at ISIS. The sample (~0.50 g) was contained in a 6 mm diameter vanadium can. The instrument D2b at ILL Grenoble was used to collect constant-wavelength ($\lambda = 1.5938$ Å) neutron powder diffraction data on sample G at a temperature of 2 K in an applied magnetic field of 0, 10, and 50 kOe, and then at temperatures of 24, 50, 140, and 200 K in a field of 50 kOe. Approximately 4 g of sample were contained in a vanadium can of diameter 5 mm which was mounted on D2b in an Oxford Instruments cryomagnet. Each data collection covered the angular range $5 \le 2\theta$/deg ≤ 140 with a step size of $\Delta 2\theta = 0.05°$. All the diffraction data reported in this paper were analyzed by the Rietveld method[6] as implemented in the GSAS[7] program package. A shifted Chebyschev polynomial was used to fit the background level in all cases. It was not possible to refine the temperature factors for the Mn/Rh site to chemically sensible values because of the low mean nuclear scattering length that results from a 3:2 Mn:Rh distribution. The temperature factors for this site were therefore held fixed at zero. Weak Bragg reflections attributable to the sample containers were observed in both the constant wavelength and time-of-flight data and vanadium was therefore included as a second phase in the analyses. Inspection of the data collected on sample G revealed that, in the period (several months) between the initial characterization and the present investigation, the La_2O_3 impurity present in the original sample had been converted to $La(OH)_3$, which was consequently included as a minority phase.

Results

The X-ray and neutron diffraction patterns of samples T and E were consistent with those expected from a monophasic, tetragonal K_2NiF_4 phase with space group *I*4/*mmm*. Rietveld analysis of the neutron diffraction data collected on GEM resulted in the structural parameters listed in Table 1 and Table S1; the corresponding parameters derived previously for sample G are included in the table for comparison purposes. The temperature dependence of the molar magnetic susceptibility of samples T and E is shown in Figure 1. Their behavior is quantitatively different, but qualitatively similar in that neither sample obeys the Curie−Weiss law, characteristic of a paramagnet, over the measured temperature range. However, although the inverse susceptibility is a nonlinear function of temperature, it is clear from Figure 1 that any attempt to derive a Weiss constant (θ) in the high-temperature region would result in a positive value; this is indicative of ferromagnetic intercation interactions. In both cases, hysteresis is apparent below ~220 K and the gradient of the inverse susceptibility increases markedly above this temperature. A maximum is observed in the ZFC susceptibility at 13 K. Sample G showed[4] the same low-temperature transition, although the onset of hysteresis and the change in gradient occurred at a somewhat lower temperature (~180 K).

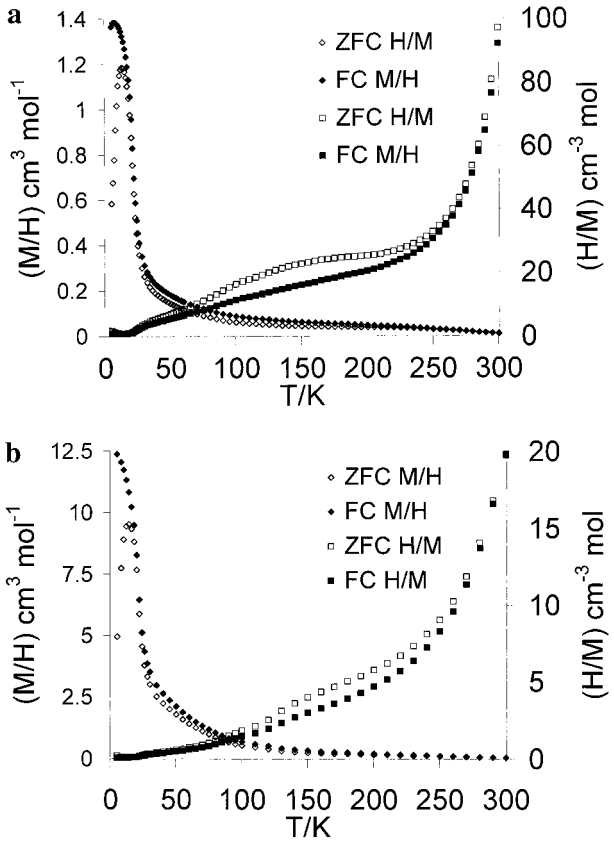

Figure 1. Temperature dependence of the molar magnetic susceptibility of $La_{0.8}Sr_{1.2}Mn_{0.6}Rh_{0.4}O_4$: (a) sample T and (b) sample E.

Attempts to analyze the neutron diffraction data collected on sample G in a magnetic field of 10 kOe at 2 K were unsuccessful when only nuclear scattering was considered. No additional Bragg peaks, indicative of a change in symmetry or unit cell size, were observed, and we therefore postulated that the atomic magnetic moments of the Mn/Rh cations order ferromagnetically in an applied field. Calculations based on this model resulted in good agreement between the observed and calculated

(5) Blundell, S. J. *Contemp. Phys.* **1999**, *40*, 175.
(6) Rietveld, H. M. *J. Appl. Crystallogr.* **1969**, *2*, 65.
(7) Larson, A. C.; von-Dreele, R. B. General Structure Analysis System (GSAS), Los Alamos National Laboratories, Report LAUR 86-748, 1990.

Table 2. Structural Parameters for $La_{0.8}Sr_{1.2}Mn_{0.6}Rh_{0.4}O_4$ (Sample G) as a Function of Applied Field and Temperature

H (kOe)	*T* (K)	*a* (Å)	*c* (Å)	*z* (Sr/La)	*z* (O1)	Mn/Rh−O1 (Å)	Mn/Rh−O2 (Å)	*M* (μ_B per Mn)	ϕ (deg)	R_{wpr} (%)	χ^2
0	2	3.88273(9)	12.4789(3)	0.35888(8)	0.1642(1)	2.049(1)	1.94136(4)			5.8	1.9
10	2	3.88285(8)	12.4789(3)	0.35888(7)	0.1644(1)	2.051(1)	1.94143(4)	2.55(9)	45(4)	5.5	2.2
50	2	3.88313(8)	12.4781(3)	0.35884(7)	0.1644(1)	2.052(1)	1.94156(4)	3.38(7)	41(2)	5.5	2.2
50	24	3.88320(8)	12.4780(3)	0.35884(8)	0.1646(1)	2.053(1)	1.94160(4)	3.21(8)	42(3)	5.6	2.5
50	50	3.88299(9)	12.4792(3)	0.35886(7)	0.1643(1)	2.050(1)	1.94150(4)	2.3(1)	41(5)	5.4	2.1
50	140	3.88381(8)	12.4891(3)	0.35885(7)	0.1644(1)	2.053(1)	1.94190(4)			5.4	2.1
50	200	3.88505(8)	12.4989(3)	0.35873(7)	0.1643(1)	2.054(1)	1.94253(4)			5.3	2.0

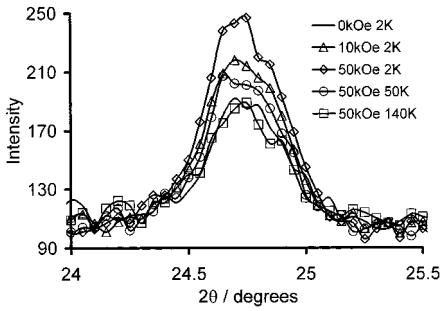

Figure 2. Intensity of the 101 reflection of $La_{0.8}Sr_{1.2}Mn_{0.6}Rh_{0.4}O_4$ as a function of applied magnetic field and temperature.

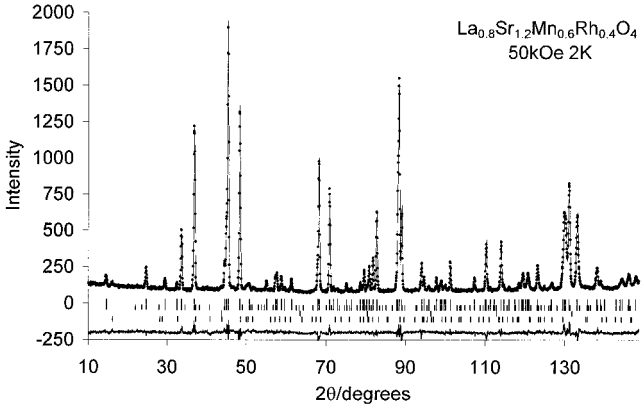

Figure 3. Observed, calculated, and difference neutron diffraction profiles of $La_{0.8}Sr_{1.2}Mn_{0.6}Rh_{0.4}O_4$ in 50 kOe at 24 K. Reflection positions are marked by vertical bars for, in descending order, nuclear scattering, magnetic scattering, $La(OH)_3$, and V.

diffraction patterns. The refined structural parameters are listed in Table 2 and Table S2 (Supporting Information); the use of a powder sample limits the information that can be deduced about the ordered moment to the magnitude (*M*) and the orientation with respect to *z* (ϕ). Tables 2 and S2 also include the results obtained from the data collected in 50 kOe at 2, 24, 50, 140, and 200 K; no magnetic contribution to the Bragg scattering was apparent at 140 or 200 K. The temperature and field dependence of the 101 reflection is shown in Figure 2, and the full diffraction pattern collected at 24 K in 50 kOe is shown in Figure 3. During the course of the analysis of the data collected in 50 kOe at $2 \leq T/K \leq 50$ it became apparent that the intensities of some Bragg peaks had changed in a manner that could not be accounted for simply by refining the usual parameters together with a magnetic moment on the Mn site. Relatively high-angle reflections, for example 220 at $2\theta \sim 72°$, showed a significant increase in intensity, and other peaks decreased in intensity. After testing a number of models we concluded that these changes were best accounted for by allowing for preferred orientation parallel and perpendicular to [001]. This effect can be ascribed to movement of the magnetized powder grains within the vanadium can.

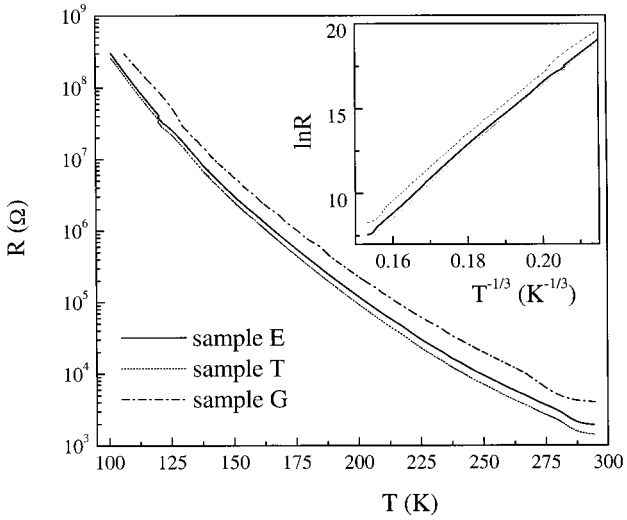

Figure 4. Temperature dependence of the resistance of $La_{0.8}Sr_{1.2}Rh_{0.4}Mn_{0.6}O_4$. The inset show the logarithm of resistance as a function of $1/T^{1/3}$.

The temperature dependence of the resistance of the $La_{0.8}Sr_{1.2}Rh_{0.4}Mn_{0.6}O_4$ samples is shown in Figure 4. Below ~100 K, the resistance becomes too large to be measured with our apparatus. All samples show insulating behavior with an activation energy of $E_A = 0.21 \pm 0.05$ eV in the region 200−300 K. The resistance can be fitted over the entire temperature range by a two-dimensional variable-range hopping law, $\rho = \rho_0 \exp(T_0/T)^{1/3}$ (see inset of Figure 4). This suggests that the electron transport is dominated by transport within the perovskite layers. The parameter T_0 varies slightly from one sample to another: $T_0 = 8.06 \times 10^6$ K for sample E, $T_0 = 8.29 \times 10^6$ K for sample T, and $T_0 = 7.86 \times 10^6$ K for sample G. The small difference between these values may indicate slightly different localization lengths and hopping distances in the different samples (localization length is proportional to $T_0^{-1/2}$ [8]). The field dependence of the resistivity for our $La_{0.8}Sr_{1.2}Rh_{0.4}Mn_{0.6}O_4$ samples is shown in Figure 5a. The maximum values of magnetoresistance in 14 T and at the lowest possible measured temperature (108 K) reached ~57% for all the samples. In the high-temperature region ($T > 100$ K), the magnetoresistance (shown for sample E) follows $\Delta\rho/\rho(0) = C(M/M_s)^2$ [9] with $M_s = 1.803\ \mu_B$ per formula unit (corresponding to 3 μ_B/Mn). This relationship, nominally valid only above the magnetic ordering temperature, accounts for the data at all temperatures when $(M/M_s) < 0.2$ (Figure 5b). However, the value of *C* that we obtain is not constant as found in other materials [9] but decreases as the temperature increases to 200 K (Figure 5b inset). This reduction might be indicative of a diminution in

(8) Mott, N. F.; Davis, E. A. *Electronic Processes in Noncrystalline Materials*, 2nd ed.; Oxford University Press: Oxford, 1979.

(9) Urushibara, A.; Moritomo, Y.; Arima, T.; Asamitsu, A.; Kido, G.; Tokura, Y. *Phys. Rev. B* **1995**, *51*, 14103.

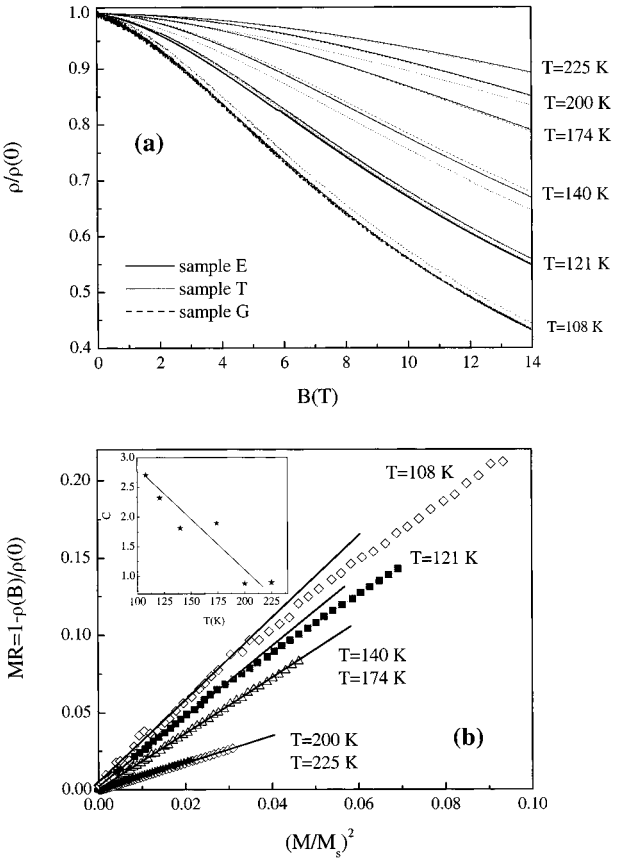

Figure 5. (a) The field dependence of the reduced resistivity, $\rho/\rho(0)$, at different constant temperatures for $La_{0.8}Sr_{1.2}Rh_{0.4}Mn_{0.6}O_4$. (b) Magnetoresistance against the square of reduced magnetization ($\Delta\rho/\rho(0) = C(M/M_s)^2$ where $M_s = 1.803\ \mu_B$ per formula unit for sample E). The inset show the variation of C with temperature.

the degree of spin correlation as the system passes from a state with short-range ordering to a paramagnetic phase ($T > \sim 220$ K).

Zero-field muon spin relaxation (μSR) data were collected on all samples, but we shall discuss only the data on samples E and G. (Data on sample T gave results intermediate between E and G, but only a limited data set with poor statistics was collected.) The μSR data can be fitted over the entire temperature range to a functional form

$$A(t) = A_r \exp(-\lambda t)^{\beta} + A_{bg}$$

where A_r is the relaxing asymmetry, λ is the relaxation rate, β is the shape parameter, and A_{bg} is a temperature-independent background parameter. We observe a sudden drop in A_r (Figure 6c) at $\sim$20 K, corresponding to a freezing of the Mn spins on the muon time scale. This behavior is correlated with a peak in the relaxation rate λ associated with the critical slowing down of the local field fluctuations (Figure 6b). Below 20 K, the relaxation rate stays constant, indicating some slow dynamics which are strongly sample dependent. The exponent β (Figure 6a) changes gradually from a value close to 1 at $T > 200$ K to $^1/_3$ below 20 K. This effect has been observed previously for spin glass systems[10] and indicates the presence of a broad distribution of relaxation times below the freezing temperature. There is a noticeable decrease in the parameter β at the

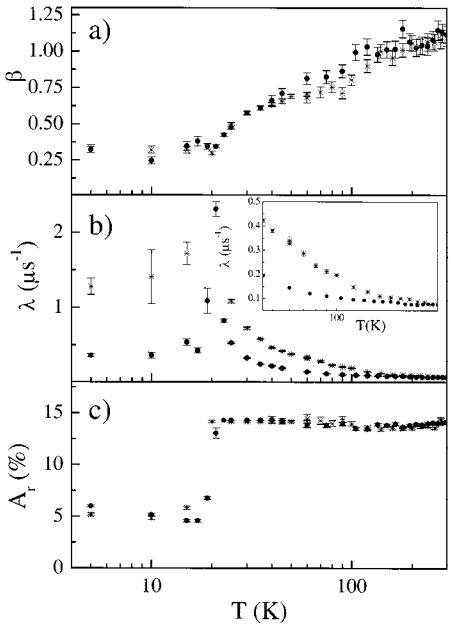

Figure 6. Temperature dependence of the μSR parameters: exponent β, relaxation rate λ, and the relaxing asymmetry A_r for samples E ($\times$) and G (●). The fitting procedure is described in the text.

temperature ($\sim$180 K) below which the relaxation rates (λ) for samples E and G begin to diverge.

Discussion

The crystallographic data presented in Table 1 establish that, averaged over the length scale sampled in a neutron diffraction experiment, the $n = 1$ RP phases contained in samples T, E, and G are not significantly different. However, sample G is known to contain unreacted $La_2O_3/La(OH)_3$ and, given the nature of the solid-state synthesis used in the preparation, the composition of the $n = 1$ phase cannot be the ideal $La_{0.8}Sr_{1.2}Mn_{0.6}Rh_{0.4}O_4$. No impurity was detected in samples T and E, and the composition of the $n = 1$ phase therein is likely to approach the ideal stoichiometry. This compositional variation could account for the difference between the magnetic susceptibility of sample G and those of samples T and E. However, the marked difference between the susceptibility of sample T and that of sample E, both apparently monophasic, suggests that other factors are also involved, for example intergrowths which perturb the microstructure of the material; a study by electron microscopy would be needed to resolve these issues. Despite the differences in the susceptibilities of the three samples, their temperature dependencies do have important features in common. In each case the gradient changes and a small hysteresis becomes apparent at $\sim$200 K and, in a measuring field of 100 Oe, there is a maximum in the ZFC susceptibility at $\sim$13 K. We shall compare the behavior of these three samples again below when we discuss the results of our magnetotransport and μSR measurements.

The magnetization data collected previously on sample G lead us to postulate that strong ferromagnetic coupling exists within the Mn/RhO_2 layers which lie perpendicular to [001], and that each sheet develops a spontaneous magnetization when 2D ordering occurs at 180 K, with the resultant magnetic moments being aligned by the applied magnetic field in the magnetometer; saturation was approached in 50 kOe at 5 K. No magnetic Bragg scattering was seen in a neutron diffraction experiment carried out at 2 K in zero applied field, although there was an increase in the diffuse scattering under certain low-angle reflections (101

(10) Campbell, I. A.; Amato, A.; Gygax, F. N.; Herlach, D.; Schenk, A.; Cywinski, R.; Kilcoyne, S. H. *Phys. Rev. Lett.* **1994**, *72*, 1291.

but not 002) on cooling from 290 to 2 K. This was taken to be further evidence of 2D short-range magnetic ordering. Our latest neutron diffraction results show that application of an applied field of 10 kOe is enough to increase the length scale of spin correlation along [001] and so produce long-range ferromagnetic order, and that a field of 50 kOe induces a moment of 3.38(8) μ_B per Mn, close to the saturation value (3.66 μ_B) expected for Mn in a mean oxidation state of 3.33 and larger than the value of 2.50 μ_B per Mn that we measured for sample G by magnetometry. The difference presumably arises from a failure to align all the magnetic moments in the bulk measurement. The orientation of the ordered magnetic vectors in the neutron diffraction experiment can be interpreted in two ways, which reflect the competition between the external magnetic field and the crystalline anisotropy. If the former dominates, then we expect the ferromagnetically coupled atomic moments in every powder grain to line up along the axis of the cryomagnet. The spin direction relative to the unit cell axes will then be different in each grain, lying anywhere between [001] and [100]. The data analysis described above then produces an imprecise description of the magnetic structure, with the spin directions listed in Table 2 being average values. Alternatively, if the applied field serves to induce long-range magnetic order, but the orientation of the ordered spins is determined by the anisotropy of the crystal and the electronic structures of the Mn cations, then the spin direction will be the same in every grain and the tabulated angles (ϕ) have a physical meaning. Our data do not allow us to distinguish between these two cases, but trial refinements showed that the magnitude of the refined magnetic moment is insensitive to changes in the spin direction and hence to the choice of model. The most striking structural change that occurs on applying a magnetic field at 2 K is the increase in the unit cell parameter *a*, and consequently the distance Mn/Rh−O2; the concomitant decrease in *c* is not significant at the 3σ level. We return to this observation below.

The results of our μSR experiments are consistent with those from diffraction and magnetometry. It is clear from the behavior of all the parameters plotted in Figure 6 that the local magnetic field at the muon site is static below a relatively sharp transition which occurs at 20 K. However, the data do not tell us whether the static field is associated with long-range or short-range magnetic ordering. We assume that this transition corresponds to the spin freezing observed at a slightly lower temperature by magnetometry, and which neutron diffraction has proved to involve only short-range ordering in the absence of a magnetic field. As was the case with the magnetic susceptibilities, the magnitude of the relaxation frequency (λ) observed by μSR is sample dependent, although the transition temperature is not. The behavior of λ below 20 K contrasts sharply with that observed[11] in the Rh-doped perovskite $La_{1.5}Sr_{0.5}MnRhO_6$, where the relaxation frequency fell rapidly to zero below the 3D ferromagnetic ordering temperature (120 K). The sample dependence of λ is apparent below ~200 K, the same temperature region where the gradient of the inverse magnetic susceptibility changes markedly. Furthermore, the parameter β (Figure 6) decreases below a value of unity below this temperature, suggesting that more than one relaxation mechanism is operating in the low-temperature regime. These observations are all consistent with the idea that sample-dependent short-range spin ordering is significant below ~200 K. The value of β below 20 K is close to the value of $^1/_3$ predicted by Campbell et al[10] for spin glasses.

All the data collected on $La_{0.8}Sr_{1.2}Mn_{0.6}Rh_{0.4}O_4$ lead to a picture of a material in which the high-temperature paramagnetism is modified below ~200 K by the increasing significance of 2D ferromagnetic short-range spin interactions within the perovskite sheets perpendicular to [001]. At lower temperatures (~20 K), in a weak or zero magnetic field, the spins freeze in a glassy state as they do in $La_{1-x}Sr_{1+x}MnO_4$ for $0.2 \le x \le 0.5$ ($T_g \sim 16$ K for $x = 0.3$[12]). We believe that in the case of $La_{0.8}Sr_{1.2}Mn_{0.6}Rh_{0.4}O_4$ this freezing is 3D in nature, and that spins in neighboring layers no longer fluctuate with respect to each other, but nor do they show any long-range correlation. This hypothesis is supported by the temperature dependence of the spin fluctuations as probed by the μSR relaxation parameter β. In this work we have used three samples, all of which would satisfy any of the criteria normally used by solid-state chemists to establish sample quality. However, the details of the magnetic behavior of this material are strongly sample dependent, suggesting a very high sensitivity to changes in composition or microstructure. The electronic properties are also very sensitive to the application of a magnetic field. Although the material is a semiconductor at all measured temperatures, it does show (Figure 5) an increasingly large negative magnetoresistance below 200 K, that is in the region where short-range spin ordering is thought to occur. Indeed, the unexpected temperature dependence of the parameter *C* is further evidence for the presence of short-range ordering below ~200 K. Furthermore, the neutron diffraction data show that the application of a magnetic field at temperatures up to 50 K (that is, above the glass transition temperature) induces long-range 3D spin alignment in this phase. It is likely that the magnetoresistance stems from the same source, that is it is caused by the field enhancing the degree of 2D short-range spin alignment which occurs spontaneously in zero field below ~200 K, and introducing correlations in the third dimension, that is along [001]. The observation of magnetoresistance ($\rho/\rho_0 \sim 0.95$) in 5 T at 140 K demonstrates that it is not necessary to induce long-range spin ordering to see an effect, although the magnitude clearly increases on cooling.

The behavior of $La_{0.8}Sr_{1.2}Mn_{0.6}Rh_{0.4}O_4$ is very different form that of other two-dimensional $n = 1$ RP oxides. We have argued previously[11] in discussing the properties of perovskite phases that the vacant e_g orbitals associated with the Rh^{3+} cation play an important role in determining the electronic properties of mixed Mn/Rh metal oxides and it is likely that these orbitals are involved in the magnetic interactions on the disordered transition metal sublatttice in the phase presently under discussion. Although both ferromagnetic and antiferromagnetic interactions are expected to be present in undoped $La_{1-x}Sr_{1+x}MnO_4$, the former do not become dominant when the oxidation state of Mn is varied. However, the Rh-doped samples do show clear evidence of strong ferromagnetic coupling, although a magnetic field must be applied in order to induce spin-alignment over long distances. One possible explanation of these observations follows from an earlier discussion of anisotropic magnetoelastic phenomena in $n = 2$ RP manganites.[13] The small but significant increase in the unit cell parameter *a* that occurs when a magnetic field is applied will lead to a reduction in the tetragonal distortion at the transition metal site and a lowering in energy of the x^2-y^2 band. Assuming that the bands are sufficiently broad to overlap, this will in turn lead to an increase in the occupation of the x^2-y^2 band at the expense of the z^2 band

(11) Coldea, A. I.; Marshall, I. M.; Blundell, S. J.; Singleton, J.; Noailles, L. D.; Battle, P. D.; Rosseinsky, M. J. *Phys. Rev. B* **2000**, *62*, R6077.

(12) Moritomo, Y.; Tomioka, Y.; Asamitsu, A.; Tokura, Y. *Phys. Rev. B* **1995**, *51*, 3297.

(13) Kimura, T.; Tomioka, Y.; Asamitsu, A.; Tokura, Y. *Phys. Rev. Lett.* **1998**, *81*, 5920.

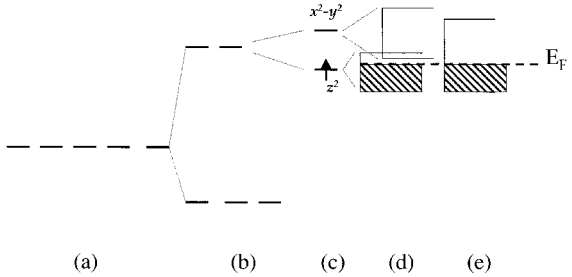

Figure 7. Band structure of $La_{0.8}Sr_{1.2}Rh_{0.4}Mn_{0.6}O_4$: the degeneracy of five d orbitals (a) is partially removed (b) by a field of O_h symmetry and reduced further (c) by a tetragonal distortion. Cation−oxide−cation interactions broaden (d) the d levels into overlapping bands of finite width and application of a magnetic field lowers (e) the x^2-y^2 band, increasing its occupancy and stabilizing a ferromagnetic state. The shading and dashed line in parts d and e indicate the occupied states and Fermi energy which are assigned on the basis of complete spin polarization within the e_g bands.

(Figure 7) and, given that the t_{2g} orbitals are half-filled, to an increase in the strength of the ferromagnetic coupling in the 2D perovskite sheets. The presence of Rh cations with empty e_g levels derived from 4d orbitals (which have a relatively large radial extent) will increase the width of the x^2-y^2 band relative to that in a Mn-only system and will thus also enhance electron transfer and hence ferromagnetic coupling. Furthermore, the filled t_{2g} orbitals of Rh^{3+} will block the antiferromagnetic superexchange between the half-filled t_{2g} orbitals of $Mn^{3/4+}$ cations. The net effect of Rh-doping is thus to weaken antiferromagnetic coupling and to promote ferromagnetism, apparently to a point where the changes in band structure brought about by the application of a magnetic field are sufficient to induce long-range ferromagnetic ordering. It follows from these arguments that the consequences of diluting the Mn sublattice in magnetoresistance materials with a diamagnetic cation are highly dependent on the electronic structure of the dopant; $3d^{10}$ Ga^{3+} would not be expected to produce the behavior described above. Given that no oxide with the K_2NiF_4 structure has previously been shown to order ferromagnetically, we hope that this fascinating behavior may lead to the discovery of new colossal magnetoresistance materials with the $n = 1$ RP structure.

Acknowledgment. We are grateful to EPSRC and ORS for funding, and to T. Hansen (ILL) and P. G. Radaelli and F. Pratt (both ISIS) for experimental assistance.

Supporting Information Available: Tables listing displacement parameters for $La_{0.8}Sr_{1.2}Mn_{0.6}Rh_{0.4}O_4$ at 290 K and for $La_{0.8}Sr_{1.2}Mn_{0.6}Rh_{0.4}O_4$ (sample G) as a function of applied field and temperature (PDF). This material is available free of charge via the Internet at http://pubs.acs.org.

JA010958+